Korean J. Chem. Eng., 38(4), 816-825 (2021)
DOI: 10.1007/s11814-020-0731-y

pISSN: 0256-1115
eISSN: 1975-7220

A comparison between ferrochrome slag and gold mine tailings based geopolymers as adsorbents for heavy metals in aqueous solutions: Analyzing reusability and sustainability

Thabo Falayi† and Bolanle Deborah Ikotun

Department of Civil and Chemical Engineering, University of South Africa, Johannesburg 1710, South Africa
(*Received 27 August 2020 • Revised 8 December 2020 • Accepted 14 December 2020*)

Abstract−Ferrochrome slag (FeCr-GP) and gold mine tailings (GMT-GP) based geopolymers were synthesized and used as adsorbents of heavy metals in aqueous solutions. Batchwise adsorption experiments were used to determine the effect of solid loading (S/L), temperature and time on the adsorption of Cu, Ni and Mn. X-ray diffraction studies showed that GMT-GP was amorphous with calcium aluminium silicate hydrate as the geopolymerization product leading to an increased surface area while GMT-GP had a significant reduction in the intensity of crystalline peaks as compared to the precursor. FeCr-GP could adsorb above 99% of the metal ions (Cu^{2+}, Ni^{2+} and Mn^{2+}) in solution with an initial metal concentration of 400 ppm at 298, while GMT-GP could only adsorb at least 98% of the metal with an initial metal concentration of 200 ppm. The adsorption was accompanied by a pH rise from 2.3 to 4.5 and 4.8 for GMT-GP and FeCr-GP, respectively. The maximum adsorption capacity of FeCr-GP was double that of GMT-GP. FeCr-GP could be desorbed using HCl and reverse osmosis water and could be used for a further three cycles without significant loss in adsorbing ability, while desorption of GMT-GP resulted a reduction in adsorption capability.

Keywords: Gold Mine Tailings, Ferrochrome Slag, Geopolymer, Desorption, Adsorption, Isotherm

INTRODUCTION

Water is a necessary component of life. The current and frequent droughts in Southern Africa [1] necessitate the need for research in the recycling of wastewater. One of the major contaminants of water is the discharge of industrial effluent into streams. The surface water is then contaminated with heavy metals, surfactants, dyes and radionuclides [2,3]. Water pollution is known to cause a number of maladies and heavy metals have been shown to be carcinogenic [4].

There are several methods for the removal of metals from waste water. The most common and cheap method is adsorption [5]. Various adsorbents can be used, which include activated carbon, clays and fly ash [6]. In recent times, geopolymers have received attention as alternative adsorbents for water purification [7]. Geopolymers are solid/amorphous materials which are synthesized from alkali activation of an aluminosilicate material [8]. Geopolymers have been shown to possess high chemical resistance, high thermal stability and high durability. They are eco-friendly in that they can be synthesized at low temperature (<100 °C) [9]. The negative charges on tetrahedral frameworks of geopolymers are usually balanced by alkali or alkaline earth cations such as Na^+ or K^+ depending on the alkali solution used [3]. The cations can then be exchanged with metals in solution, thus resulting in the metal removal potential of geopolymers. The other removal mechanism that has been postulated includes physisorption in the absence of ion exchange [8]. Physisorption is the preferred mechanism as it offers adsorbent regeneration potential [10]. The use of geopolymers from industrial waste is critical for sustainable development. Waste based geopolymers are thus important in that they are secondary resources which can be used to meet a global resource scarcity. The use of waste based geopolymers allows for valorization of pollutants, thus satisfying the dictates of industrial ecology.

A number of geopolymers have been used as adsorbents, including bentonite/Fe_3O_4 geopolymer with over 92% removal efficiency of Cu, Pb, Cd and Hg [7], a rice husk/ash, palm oil fly ash, metakaolin and slag composite geopolymer with over 85% removal efficiency of methylene blue dye [8], a metakaolin based magnetic geopolymer for the removal of green and procion red [11]. The proposed removal mechanism is thought to be ion exchange [12], although precipitation is also possible due to high pH of some geopolymers.

Geopolymers can be synthesized from precursors that contain Si and Al. It is well known that gold mine tailings (GMT) and ferrochrome (FeCr) slag contain considerable amount of Si and Al and can be utilized as precursors for the synthesis of geopolymers [13, 14]. Stabilization of FeCr slag and GMT via geopolymerization is important in that it reduces the metal leachability of these materials into the environment [13,14].

The overwhelming precursors for geopolymer adsorbents used in wastewater treatment include blast furnace slag, fly ash, metakaolin and rice husk ash [15-17]. In recent times, attention has also focussed on other wastes as precursors, and these include pyrophyllite mine waste and dolochar ash [18,19]. The resulting geopolymers have been shown to adsorb over 98% of Co, Cd, Ni and Pb in solution. Furthermore, in the review by Luukkonen et al. [16], less than 25% of the research focussed on the regeneration of the

†To whom correspondence should be addressed.
E-mail: tfalayi@gmail.com

adsorbents; regeneration and reusability are critical in the sustainable use of a resource. In this research the use of gold mine tailings and ferrochrome slag based geopolymers as adsorbents was investigated. The use of the two industrial wastes is an endeavour to satisfy the demands of a circular economy where resources are kept within the economic cycle as much as possible. The two geopolymers are compared to each other's performance to verify the effect of precursor/geopolymer type on the removal efficiency. Furthermore, the regeneration coupled with reusability was investigated to satisfy the demands of sustainability. To the best of our knowledge, there has been no recorded ferrochrome slag based geopolymer used as an adsorbent in literature; thus, this geopolymer may be a first. Gold mine tailings based geopolymers have been referenced once in literature [20], for the removal of Pb^{2+}, and thus this paper seeks to add more heavy metals which can be removed using gold mine tailings based geopolymers. Though geopolymers have been shown to be promising adsorbents, more research is needed over the whole range of possible precursors [16]. This research paper therefore seeks to introduce a new material (ferrochrome slag and gold mine based geopolymer) as a possible adsorbent for heavy metals in wastewater.

MATERIALS AND METHODS

1. Materials

Synthetic water was used as an effluent. The use of synthetic water is generally accepted as a first step in the determination of the effectiveness of the proposed geopolymer adsorbent [16]. Appropriate amounts of $MnSO_4{\cdot}H_2O$, $NiSO_4{\cdot}5H_2O$ and $CuSO_4{\cdot}5H_2O$ were added to reverse osmosis (RO) water to make a 1,000 ppm stock solution. All adsorption experiments were carried out with a heavy metal solution at a pH of 2.3 to mimic acid mine drainage obtained in South Africa [6]. FeCr was obtained from a ferrochrome smelter in South Africa. The major elements by weight were 47% Si, 10.9% Al, 14.7% Cr and 9.9% Fe. GMT was obtained from a mine tailings dam in the West Rand area of South Africa. The major GMT elements were 65% Si, 7.0% Al, 7% Fe and 5.2% Mg.

2. Methodology

2-1. Synthesis of Geopolymer

The GMT geopolymer (GMT-GP) was synthesized using the author's previous optimization work on the synthesis of GMT geopolymers [13]. The oven dry GMT was mixed with an alkaline solution (10 M KOH with a potassium aluminate to KOH ratio of 2) using a liquid to solid ratio (L/S) of 0.26. The resultant paste was poured into a 100×100×100 mm mould. The filled mould was hand shaken for 3 min to remove any air bubbles in the paste. The cast was cured at 100 °C for 120 h. At the end of the curing period the geopolymer was milled to less than 75 μm and washed with RO water till the washings were at a pH of 7. The now neutral geopolymer was then oven dried for 24 h at 105 °C and subsequently crushed to less than 75 μm before adsorption experiments.

The FeCr slag geopolymer (FeCr-GP) was synthesized using the author's previous optimization work on the synthesis of FeCr slag geopolymers [14]. Oven dry FeCr slag was mixed with an alkaline solution (10 M KOH with a ratio of potassium aluminate (KA) to KOH of 1.25. The liquid to solid ratio (L/S) was 0.26. The resultant paste was poured into a 100×100×100 mm mould. The filled mould was hand shaken for 3 min to remove any air bubbles in the paste. The cast was cured for 28 d at room temperature. At the end of the curing period the geopolymer was crushed to less than 75 μm and washed with RO water till the washing were at a pH of 7. The now neutral geopolymer was oven dried for 24 h at 105 °C and subsequently crushed to less than 75 μm before adsorption experiments. The two geopolymers (GMT-GP and FeCr-GP) were chosen because they had the best durability, highest unconfined compressive strength (structural integrity), lowest metal leachability and highest resistance to alternate wet and dry cycles [13,14].

3. Adsorption Experiments

All adsorption experiments were carried out in a thermostatic batch vessel in triplicate.

3-1. Effect of Solid Loading

0.1 to 1.4 g of FeCr-GP was added, respectively, to 100 ml of synthetic wastewater containing 100 ppm Cu, 100 ppm Ni and 100 ppm Mn at a pH of 2.3 to reflect the average composition of acid mine drainage in South Africa [6]. The mixture was agitated at 250 revolutions per minute (rpm) at 25 °C for 2 hrs. At the end of 2 h the mixture was filtered using a filter paper and the filtrate was subsequently assayed for heavy metals. The pH at the end of the agitation period was also measured. The above method was repeated with FeCr (control), GMT-GP and GMT (control). The amount of metal adsorbed per mass of adsorbent (q_t) was calculated using Eq. (1)

$$q_t = C_o - C_t \times \frac{V}{m} \tag{1}$$

where C_o is the concentration of metal (ppm) before adsorption, C_t is the concentration of the metal after a t min of adsorption (ppm), V is the volume of synthetic wastewater in liters and m is the mass of the adsorbent in g.

3-2. Effect of Initial Concentration

0.7 g (optimum solid loading from 3.1) of FeCr-GP was added to heavy metal solutions with the metal concentration varying from 100 ppm to 600 ppm. The resulting mixtures were agitated at 250 rpm and at 25 °C for 2 hrs. At the end of 2 h, the mixtures were filtered using a filter paper and the filtrates were subsequently assayed for heavy metals. The same procedure was repeated with 1.0 g (optimum solid loading from 3.1) of GMT-GP.

3-3. Effect of Contact Time and Temperature

FeCr-GP was added to 100 ml of synthetic wastewater (concentration at 400 ppm Cu, Ni and Mn) using a solid loading (SL), which gave the best removal efficiency from the effect of solid loading experiments. The mixtures were agitated at 250 rpm and at 25 °C for 30, 60, 90, 120, 150, 180, 210 and 240 mins, respectively. At the end of the respective agitation times, the mixtures were filtered using a filter paper and the filtrates were subsequently assayed for heavy metals. The above method was repeated with GMT-GP using synthetic water with metal concentration of 200 ppm Cu, Ni and Mn. The procedure was also repeated at 35 °C and 45 °C to test the effect of temperature on the adsorption of the heavy metals onto the respective geopolymers.

3-4. Desorption Studies

The metal loaded geopolymers were desorbed using reverse

osmosis water, HCl and H_2SO_4 to test for possible regeneration of the geopolymer adsorbent. The acid desorbed geopolymers were washed with RO water till the washings were at near neutral pH. The desorption efficiency was chosen as a criterion for the determination of the desorbing solution. After desorption each geopolymer was re used as an adsorbent to a fresh 100 ml of synthetic wastewater.

3-5. Statistical Analysis

All error bars were at 95% of the confidence interval, and ANOVA was used to calculate statistical variance.

4. Assaying Methods

The atomic absorption spectrometer (Thermo scientific ICE 3000 series) was used for the determination of heavy metals. X-ray fluorescence (XRF) (Rigaku ZSX primus II) was used for the determination of the elemental composition of the precursors. The precursors were ground to less than 75 μm and made into a pellet using a pneumatic compressor. The resulting pellet was then dried at 50 °C for 12 h and immediately afterwards run on the XRF machine using Si as a standard. The X-ray diffraction (Ultima IV Rigaku XRD) using a reference internal ratio (RIR) method was used for the mineralogical determination for the precursors and geopolymers. A ground sample (<75 μm) was placed on the XRD sample holder and the machine was run from 0° to 90° 2θ angle. The obtained bonds of the precursors and geopolymers were determined using Fourier transform infra-red spectrometry (FTIR) (Thermoscientific Nicolet IS10). A ground sample was placed in the FTIR sample holder and run on a KBR line. Laser diffraction (Malvern Mastersizer 2000) was used to determine particle size distribution (PSD) of the geopolymers with water as a dispersion medium.

5. Adsorption Isotherms and Kinetics

The most commonly used isotherms for heavy metal adsorption are Freundlich and Langmuir isotherms. The Freundlich isotherm is usually used for nonlinear adsorption, but is also used for multilayer adsorption on heterogeneous surfaces [21]. The linear form of the Freundlich isotherm is:

$$\ln q_t = \ln K_F + \frac{1}{n}\ln C_t \tag{2}$$

where C_t (ppm) is the concentration of the concerned metal ion after t mins of adsorption, K_F is the Freundlich constant related to adsorption intensity and q_t is the amount of metal adsorbed per amount of adsorbent. The Langmuir isotherm represents monolayer adsorption [22] with a number of assumptions that include that the adsorption sites are equally distributed, resulting in constant adsorption energy and the interaction between adsorbate molecules is negligible [23]. The linearized form of the Langmuir isotherm is:

$$\frac{C_t}{q_t} = \frac{1}{q_m \times b} + \frac{C_t}{q_m} \tag{3}$$

where C_t (ppm) is the concentration of the metal ion of concern after t mins of adsorption, q_m (mg/g) is the maximum adsorption capacity of the adsorbent, b (L/g) is a constant related to enthalpy of adsorption.

The most utilized kinetic models for adsorption are the Lagergren pseudo-first-order model and the pseudo-second-order model.

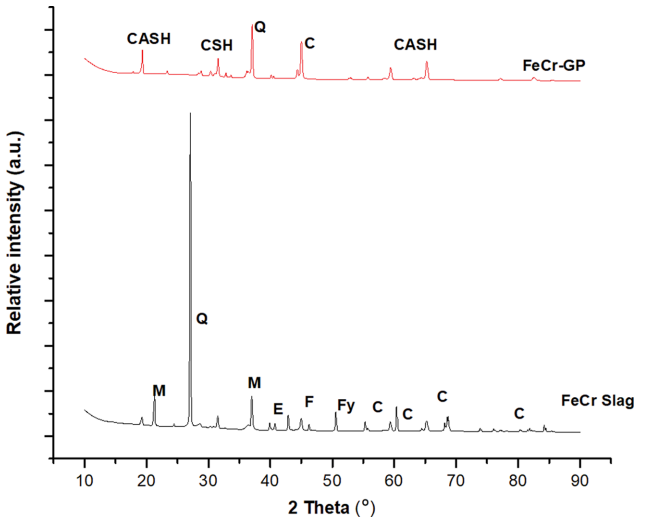

Fig. 1. XRD diffractogram of FeCr slag and FeCr-GP (M=Magnesiochromite, F=Fosterite, Fy=Fayalite, C=Chromite, E=enstatite, CASH=Calcium aluminate silicate hydrate, CSH=Calcium Silicate Hydrate).

Their linearized forms are shown in Eqs. (4) and (5), respectively.

$$\log(q_e - q_t) = \log q_e - \frac{k_1}{2.303}t \tag{4}$$

$$\frac{t}{q_t} = \frac{1}{k_2 q_e} + \frac{1}{q_e}t \tag{5}$$

where q_e is the adsorption capacity at equilibrium, k_1 and k_2 are constants. The pseudo-first-order is suitable for the first 20-30 min of adsorption [24]. The pseudo-second-order model usually gives the best estimation of adsorption capacity at equilibrium due to its small sensitivity to random experimental errors [25].

RESULTS AND DISCUSSION

1. Characterization of Geopolymers

Fig. 1 shows the XRD diffractogram of FeCr and its geopolymer represented as FeCr-GP.

The reduction in the intensity of the quartz peak for the FeCr-GP as compared to FeCr (Fig. 1) was due to the participation of quartz in the dissolution reactions [26]. The shift in the quartz peak from about 24° to about 34° was evidence of the restructuring of the mineralogy of the precursor. The geopolymer had an elevated baseline from 15° to 32°, which was evidence of the introduction of an amorphous structure into the geopolymer. The major difference between FeCr and FeCr-GP was that the geopolymer contained calcium aluminate silicate hydrate (CASH) in addition to calcium silicate hydrate (CSH) which were not present in the precursor.

There was no major difference between GMT and GMT-GP except for the reduction in intensity of crystalline peaks (Fig. 2). This may be due to dissolution of these minerals in the highly alkaline medium used for making the geopolymer paste. The GMT-GP diffractogram was similar to that of the precursor, showing that

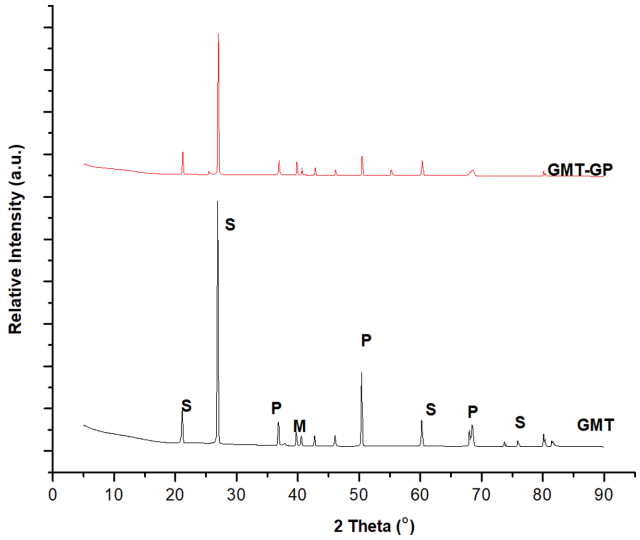

Fig. 2. XRD diffractogram of GMT and GMT-GP (S=quartz, P= pyrite, H=haematite).

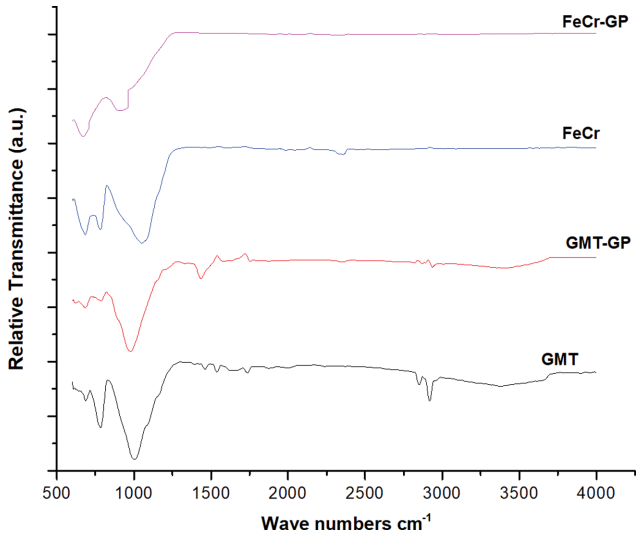

Fig. 3. FTIR spectrum of GMT, GMT-GP, FeCr and FeCr-GP.

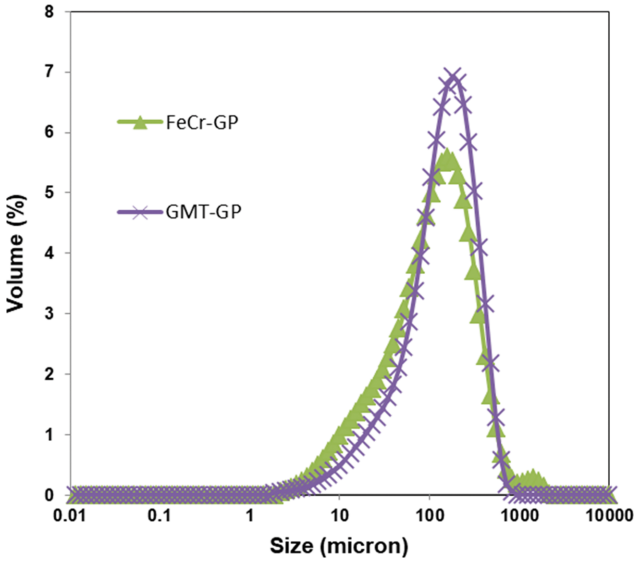

Fig. 4. Volume particle size distribution of geopolymers.

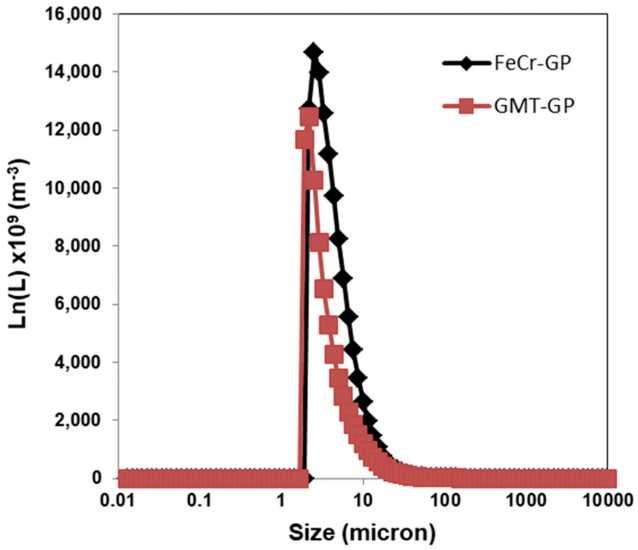

Fig. 5. Number particle size distribution of geopolymers.

the geopolymerization was not complete. Though there was absence of amorphous phases, geopolymerization should have taken place as not all geopolymers showed an amorphous structure [26,27].

The main band for GMT was centered around 1,004 cm^{-1}, which is typical of TO4 (T is aluminum or silicon) (Fig. 3). Geopolymerization of GMT led to the shifting of this band to a lower wavenumber (970.06 cm^{-1}) for GMT-GP, which showed reduction in crystallinity. The Si-O bands were resolved as the band at 784 cm^{-1} [28]. For FeCr, alumina was resolved as the band at 687.17 cm^{-1} [29]. The bands at 3,379 and 1,461 cm^{-1} were assigned to the OH group [30]. The bands around 683 and 783 cm^{-1} were resolved as metal oxides and spinels of magnesiochromite [31]. The band around 1,050 cm^{-1} was resolved as of Si-O [32,33]. The band around 1,010 cm^{-1} for FeCr shifted lower wavenumbers for FeCr-GP, which could be interpreted as an increase in the amorphous nature of the geopolymer. Laser diffraction was used to determine particle size distribution (PSD) of the geopolymers. The volume PSD was then transformed to a number density distribution with subsequent calculation of the second moment (m2), which is equivalent to the external surface area of the sample [34]. A significant volume (7%) of GMT-GP was dominated by particles whose mean size was 100 μm as compared to 5.2% for the FeCr-GP (Fig. 4). Using the number distribution (Fig. 5), FeCr-GP had a larger number of smaller particles as compared to GMT-GP, which resulted in a higher external surface area for FeCr-GP (Table 1).

The general mechanism of geopolymerization reaction is thought to occur through three stages: dissolution-coagulation, coagulation-condensation, and condensation-polymerization [35]. The first stage starts with the breakage of Si-O-T bonds, where T is either Si or Al, due to the attack by the hydroxyl ion from the alkali solu-

Table 1. External surface area of Geopolymers

Sample	GMT-GP	FeCr-GP
External surface area (m^2 m^{-3})	3.39×10^3	5.29×10^3

tion leading to formation of silanol (-T-OH) and sialate (-Si-O-) species. The coagulation-condensation stage is dominated by the accumulation of ionic species leading to polycondensation and coagulated structures. The last stage is condensation-polymerization stage where there is product. FeCr contains a considerable amount of Ca. It has been reported that Ca is involved in the activation of the geopolymer gel formation, leading to increase in strength development [36]. CaO and MgO have higher dissolution rates compared to Al_2O_3 and SiO_2, resulting in the formation of CASH [37] (Fig. 1). The incorporation of aluminate changes the Si/Al ratio, resulting in the disruption of the Si-O-Si networks by incorporation of Al, resulting in absorbance in the lower wavenumbers [37] (Fig. 3). Gold mine tailings with low Ca content, geopolymer formation is thought to be a condensation reaction between AlO^{5-}_{4-} and the SiO^{4-}_{4-} [38].

2. Effect of Solid Loading

The use of GMT and FeCr as adsorbents resulted in the leaching of metals than adsorption, which is why they were not included in Fig. 6. The removal efficiency of the respective geopolymers increased with solid loading due to increase in available sites for adsorption as the mass of the adsorbent was increased. There was no significant increase in metal removal from 0.7 to 1% m/v solid loading (S/L) for FeCr-GP as the ANOVA calculation yielded *p* value of 0.996 (p>0.05) (Fig. 6(a)). The same trend was observed for GMT-GP but within the S/L range of 1.0 to 1.4% m/v. The calculated ANOVA *p* value was 0.774 (p>0.05). The insignificant increase in metal removal could be due to metal exhaustion for FeCr-GP and GMT-GP as more than 99.6% of metals were removed.

3. Effect of Initial Concentration

There was no significant reduction in metal removal for FeCr-GP up to an initial metal concentration of 400 ppm. This may have been due to enough available sites for adsorption. At an initial concentration of 500 ppm there was a 25%, 27% and 28% reduction in metal removal for Cu, Ni and Mn, respectively (Fig. 7(a)), which may have been due to adsorption site exhaustion or adsorbent saturation. The GMT-GP experienced significant metal removal reduction at an initial metal concentration of 300 ppm (Fig. 7(b)). The higher adsorption capability of FeCr-GP can be attributed to the presence of CASH and CSH in its structure which are not present in GMT-GP (Fig. 1 and 2). CASH and CSH are associated with the amorphous structure of geopolymers which would then mean a larger surface area for metal adsorption (Table 1).

4. Effect of Time and Temperature on Adsorption

There was an increase in metal removal with time for both geopolymers (Fig. 8).The increase may be attributed to the increase of pH (Fig. 9), as it has been shown that pH plays a major role in adsorption, as there was a direct correlation between Fig. 8 and 9 [6]. The pH rise was small, suggesting that the solution was well buffered due to geopolymer washing after geopolymerization, which removed excess alkalinity. The metal uptake was quite fast in the first 30 minutes with equilibrium reached after 60 minutes. The equilibrium may be due to metal ion depletion in the solution or the exhaustion of adsorption sites. The attainment of equilibrium after 60 minutes agrees with Panda et al. [18]. The order of removal

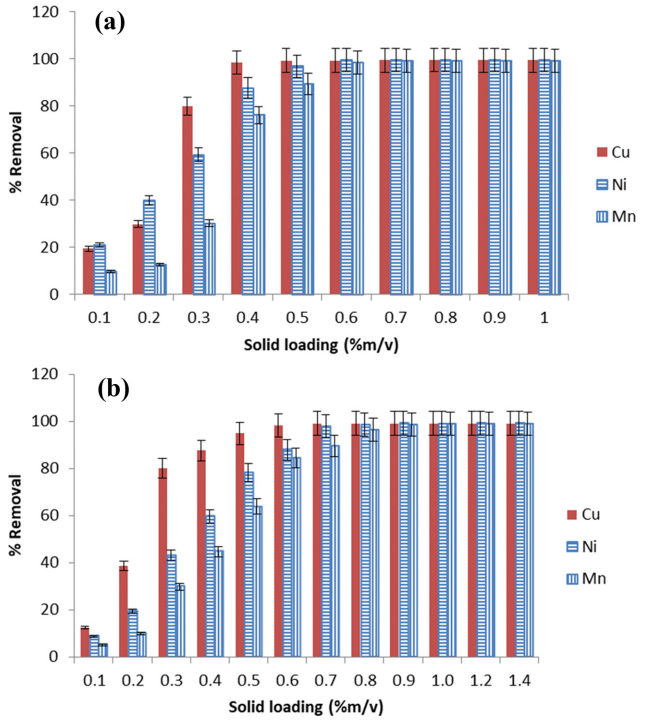

Fig. 6. Effect of solid loading on the metal removal efficiency using FeCr-GP (a) and GMT-GP (b). Agitation at 250 rpm, time at 2 h, temperature at 25 °C and 100 ppm Cu, Ni and Mn, respectively.

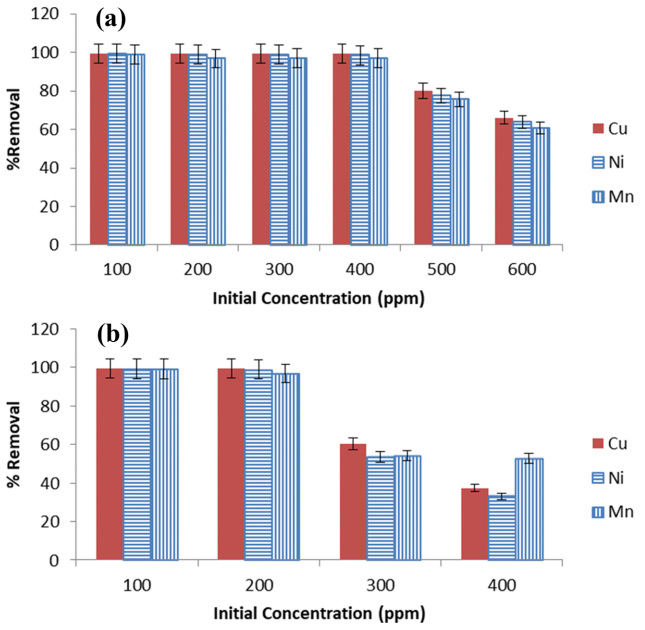

Fig. 7. Effect of initial metal concentration on the metal removal efficiency using FeCr-GP at 0.7% S/L (a) and GMT-GP at 1% S/L (b). Agitation at 250 rpm and temperature at 25 °C for 2 h.

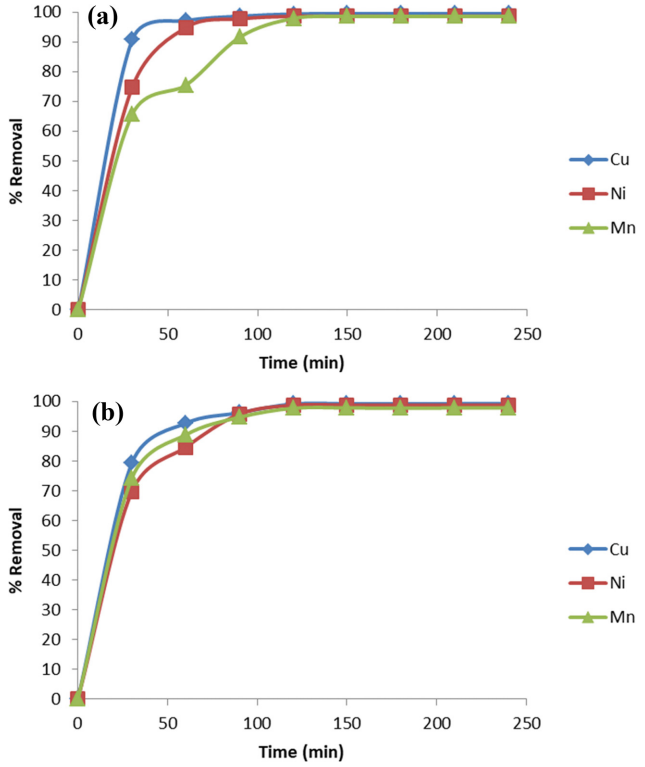

Fig. 8. Effect of adsorption time on the metal removal efficiency using FeCr-GP at 0.7% S/L and initial metal concentration of 400 ppm (a) and GMT-GP at 1% S/L and initial metal concentration at 200 ppm (b). Agitation at 250 rpm and temperature at 25 °C.

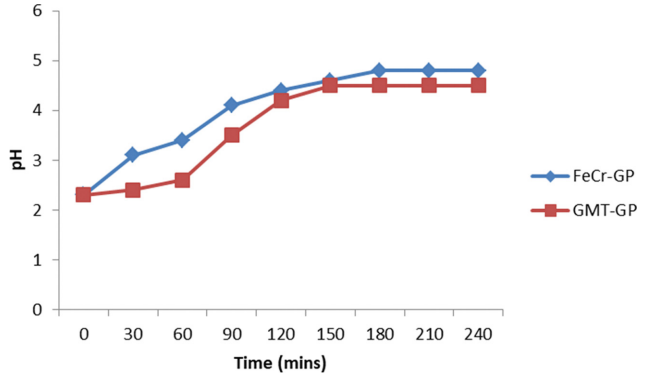

Fig. 9. Variation in pH with adsorption time FeCr-GP at 0.7% S/L and GMT-GP at 1% solid loading, agitation at 250 rpm and temperature at 25 °C.

for both geopolymers was Cu>Ni>Mn. There was no significant change in metal removal from 120 mins for both geopolymers.

There was a slight increase in adsorption capacity from 25 to 35 °C, and thereafter the increase in temperature resulted in a statistically insignificant rise in adsorption capacity (Table 2). The increase in adsorption with temperature is thought to be evidence of chemisorption [18]; however, in this study the insignificant increase would therefore support physisorption, which is also supported by the thermodynamic data (Tables 3 and 4). The insignificant increase may be because at 25 °C more than 98% of the metal ions could be adsorbed by both geopolymers.

5. Isotherms

The data for the variation in concentration at various temperatures was fitted into the two adsorption isotherms. The linearized Langmuir and Freundlich Isotherms are shown in Eqs. (3) and (2), respectively

$$\frac{C_t}{q_t} = \frac{1}{q_m \times b} + \frac{C_t}{q_m} \tag{3}$$

$$\ln q_t = \ln K_F + \ln C_t \tag{2}$$

The first criterion for choosing either model was based on the correlation coefficient (R^2) of the data. The data for Freundlich isotherm is not shown, as the R^2 was below 0.65. The adsorption of Cu, Ni and Mn onto FeCr-GP and GMT-GP, respectively, could

Table 2. Variation in adsorption capacity with temperature

Temperature (°C)	FeCr-GP adsorption capacity q_t (mg g^{-1})			GMT-GP adsorption capacity q_t (mg g^{-1})		
	Cu	Ni	Mn	Cu	Ni	Mn
25	56.88	56.36	55.42	28.35	28.20	27.67
35	57.01	56.69	56.32	28.42	28.28	27.94
45	57.07	56.69	56.69	28.48	28.38	28.13

Table 3. Langmuir isotherm and thermodynamic parameters of FeCr-GP (initial concentration at 400 ppm Cu, Ni and Mn)

	Cu			Ni			Mn		
	298.15	308.15	318.15	298.15	308.15	318.15	298.15	308.15	318.15
q_m (mg/g)	51.81	55.56	55.87	42.02	46.73	49.75	34.50	38.31	42.73
B (L/g)	3.51	30.00	59.67	1.002	1.14439	2.05102	0.16872	1	1.0
ΔG (kJ/mole)	−3.11	−8.71	−10.82	−0.05	−0.35	−1.90	−8.92	−9.34	−9.93
ΔS (J/mole)		385.17			94.76			50.78	
ΔH (kJ/mole)		111.11			28.45			6.25	
R^2	0.9996	0.9997	0.9998	0.9988	0.9993	0.9997	0.9871	0.9925	0.9987

Table 4. Langmuir isotherm and thermodynamic parameters of GMT-GP (initial concentration at 200 ppm Cu, Ni and Mn)

	Cu			Ni			Mn		
	298.15	308.15	318.15	298.15	308.15	318.15	298.15	308.15	318.15
q_m (mg/g)	22.624	25.773	27.027	20.121	22.222	25.189	15.41	20.96	24.21
B (L/g)	1.540	6.159	19.474	1.076	1.355	4.616	1.25	2.64	3.96
ΔG (kJ/mole)	−1.07	−4.66	−7.85	−0.18	−0.78	−4.05	−0.56	−2.49	−3.64
ΔS (J/mole)		339.15			193.22			153.82	
ΔH (kJ/mole)		99.98			57.87			45.17	
R^2	0.9973	0.9994	0.9999	0.9933	0.9976	0.9994	0.996	0.9958	0.9998

be modelled well using the Langmuir Isotherm (Table 3 and Table 4), which showed that these geopolymers had numerous and variant types of binding active sites [10]. Although the Langmuir isotherm is for homogeneous surfaces, it has been used to describe the adsorption onto geopolymer adsorbents [2,3,8]. This may mean that though the geopolymers are heterogeneous, the adsorption sites may relatively be evenly distributed to allow for approximation of homogeneity. There was an increase the q_m, negative value of ΔG^o and R^2 for the two geopolymers as temperature was raised from 25 °C to 45 °C. This indicated a more favorable adsorption of Ni, Cu and Mn onto the geopolymers. The positive entropy values (ΔS^o) for both geopolymers showed that there was a positive attraction between metal ions in solution and the surfaces of the geopolymers. The enthalpy of adsorption (ΔH^o) was positive, showing that the process was endothermic; this was another reason for the increase in q_m with temperature. Note that the entropy, q_m and R^2 values of FeCr-GP were higher than those of GMT-GP (Tables 3 and 4). This would then explain why the FeCr-GP saturation was at 400 ppm concentration of heavy metals while the saturation for GMT-GP was 200 ppm (Fig. 7). The sorption mechanism was typical of physisorption as the ΔG^o values both geopolymers were below −20 kJ/mol [39]. This was a good indication that the adsorption was reversible and therefore could allow for desorption and regeneration of the adsorbent, which then satisfied sustainability issues.

6. Kinetics

The adsorption data was plotted using pseudo-first and second-order kinetics. These are represented by Eqs. (4) and (5), respectively:

$$\log(q_e - q_t) = \log q_e - \frac{k_1}{2.303}t \quad (4)$$

$$\frac{t}{q_t} = \frac{1}{k_2 q_e} + \frac{1}{q_e}t \quad (5)$$

where q_e is the adsorption capacity at equilibrium, k_1 and k_2 are constants. The data for pseudo-first-order had an R^2<0.47 and was not included in Figs. 10 and 11. The data for the adsorption of Cu, Ni and Mn onto FeCr-GP and GMT-GP could be modelled well using pseudo-second-order model. Experimental and calculated q_e were compared and are shown in Table 5. The values of q_e were within 10% of each other, further proving the validity of using the pseudo-second-order to model the adsorption data.

7. Desorption and Reuse of Regenerated Adsorbent

Sustainability demands require the continued participation of a resource within the economic cycle in order to preserve and con-

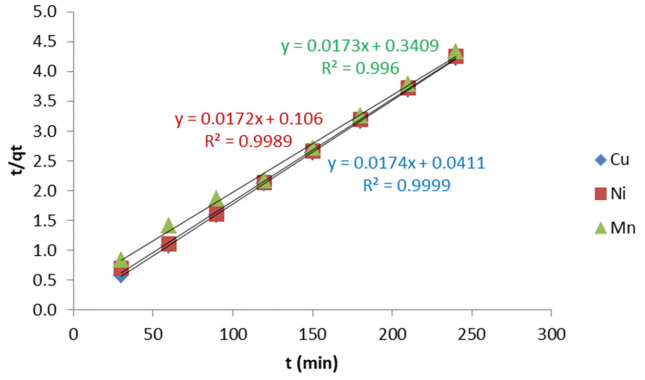

Fig. 10. Pseudo-second-order plot for FeCr-GP at 25 °C.

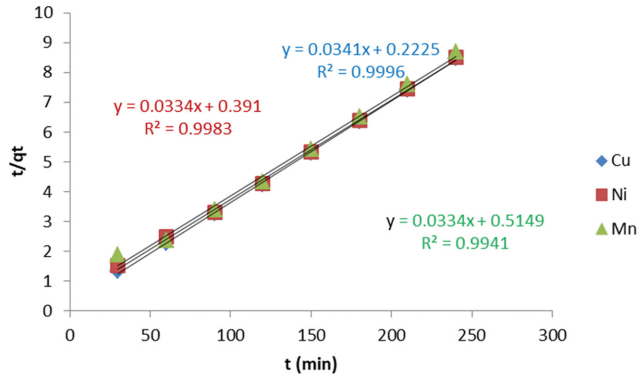

Fig. 11. Pseudo-second-order plot for GMT-GP at 25 °C.

Table 5. Comparison between calculate and experimental q_e values

	Calculated q_e (mg g^{-1})	Actual q_e (mg g^{-1})	Difference
FeCr-GP			
Cu	57.08	57.06	0.02
Ni	58.14	56.36	1.78
Mn	61.34	55.42	5.92
GMT-GP			
Cu	29.94	28.34	1.60
Ni	29.33	28.20	1.13
Mn	29.33	27.67	1.66

Table 6. Variation in metal ion recovery during desorption

	0.01 M HCl	0.02 M HCl	0.03 M HCl	0.01 M H_2SO_4	0.02 M H_2SO_4	0.03 M H_2SO_4	RO water
FeCr-GP							
Cu (ppm)	395.45	395.67	395.88	398.78	410.35	411.54	110.34
Ni (ppm)	389.67	391.24	391.34	399.56	404.56	407.45	121.23
Mn (ppm)	385.56	386.98	387.67	387.88	402.45	403.66	128.67
GMT-GP							
Cu (ppm)	198.56	198.89	198.78	199.12	211.78	211.89	60.34
Ni (ppm)	190.34	191.67	191.88	197.33	209.66	209.99	80.34
Mn (ppm)	191.34	191.67	191.89	198.34	208.59	205.88	90.67

serve resources in an environment where resource depletion abounds. One of the pillars of a circular economy is reuse and repair, and as such the metal loaded adsorbents were desorbed using H_2SO_4, HCl and reverse osmosis water.

There was no significant statistical increase in the amount of desorbed metal ions as the strength of HCl was increased for both geopolymers (Table 6). There was an increase in metal desorption with an increase in the acid strength of H_2SO_4. This was due to more H^+ ions in solution that could be exchanged with the metal ions on the adsorbent. 0.01 M HCl and 0.01 M H_2SO_4 were chosen as desorbing acids. Higher concentrations of H_2SO_4 were not chosen, as there was more than 100% recovery of metal ions from both geopolymers. This may have been due to leaching of metal ions from the geopolymer matrix. RO water could desorb 27.7%, 30.4% and 32.2% of Cu, Ni and Mn respectively from FeCr-GP, while RO water could desorb 30.3%, 40.3% and 45.6% of Cu, Ni and Mn, respectively, from GMT-GP. This further supports that the mode of sorption was physisorption. To choose between H_2SO_4 and HCl, the desorbed geopolymers were reused as adsorbents.

There was a statistically significant reduction in metal removal rate with the use of sulfuric acid as a desorbing agent for FeCr-GP ($p=0.02$), while the use of HCl resulted in statistically insignificant reduction in metal adsorption ($p=0.35$) (Fig. 12). The major cause for this was the destruction of the CASH structure of the FeCr-GP because H_2SO_4 is a stronger acid, which led to the disappearance of the CASH peak around 65° as shown in Fig. 13. The HCl desorbed FeCr-GP could be used for three cycles of desorption without any significant loss of adsorbing power (Fig. 12). Desorption using HCl resulted in at least 17% reduction in metal removal, while the use of H_2SO_4 resulted in 39% reduction in metal removal efficiency for GMT-GP. The absence of geopolymerization products from the structure of GMT-GP may have contributed to this decline. The results show the importance of microstructure in the use of a geopolymer adsorbent. The geopolymerization products (CASH and CSH) increase the adsorption capacity of the FeCr-GP (Table 5) as well as the reusability of the geopolymer adsorbent (Fig. 12). The introduction of the amorphous structure for FeCr-GP (Fig. 1) allows for an increase in the surface area available for adsorption. The amorphous structure also allows for pores that can accommodate adsorbed metal ions [18]. The negative charge associated with geopolymers allows for the improved adsorption of cations and hence the negative charge has a synergistic effect on the cation adsorption capability [40]. The absence of the amorphous structure and geopolymerization products in GMT-GP accounts for its lower adsorption capacity and lower capability to be reused (Fig. 12).

The FeCr-GP and GMT-GP exhibited q_m comparable to those in literature (Table 7). The advantage, however, of FeCr-GP is its

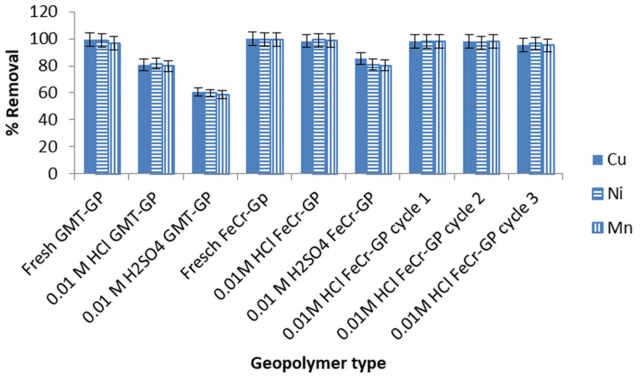

Fig. 12. Variation in metal removal with the type of desorbed geopolymer FeCr-GP at 0.7% solid loading and metal concentration of 400 ppm and GMT-GP at 1% solid loading and metal concentration of 200 ppm. Agitation at 250 rpm and temperature at 25 °C.

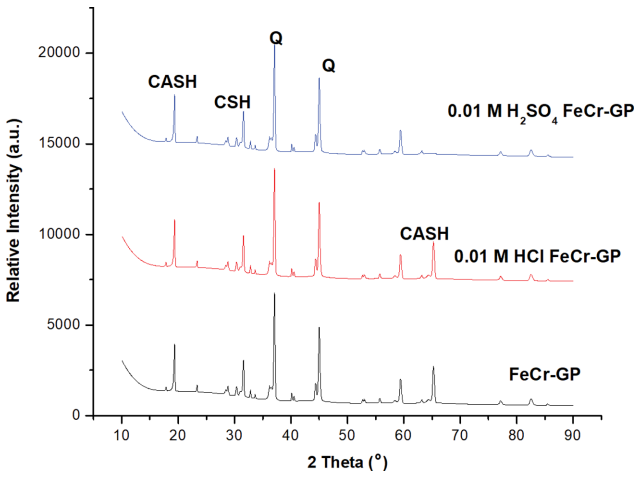

Fig. 13. XRD diffractogram of various FeCr-GP.

Table 7. Comparison with other adsorbents from literature using q_m

Metal ion/ Adsorbate	Precursor	C_o (mg L^{-1})	pH	Solid loading (g L^{-1})	q_m (mg g^{-1})	Regeneration	Reference
Cu^{2+}, Ni^{2+}, Mn^{2+}	Gold mine tailings	200 ppm	2.3	0.7	Cu^{2+}=28.35* Ni^{2+}=28.20* Mn^{2+}=27.67*	0.01 M HCl and RO water	This study
Cu^{2+}, Ni^{2+}, Mn^{2+}	Ferrochrome slag	400 ppm	2.3	1	Cu^{2+}=56.36* Ni^{2+}=56.36* Mn^{2+}=55.42*	0.01 M HCl and RO water	This study
Co^{2+}, Cd^{2+}, Ni^{2+}, Pb^{2+}	Pyrophyllite	10-50	2.2-11.5	2.5	Co^{2+}=7.18 Cd^{2+}=7.28 Ni^{2+}=7.54 Pb^{2+}=7.82	None	[18]
Co^{2+}, Ni^{2+}, Cd^{2+}, Pb^{2+}	Dolochar ash	10-50	2-12	0.5-3.5	Co^{2+}=7.18 Cd^{2+}=7.28 Ni^{2+}=7.54 Pb^{2+}=7.82	None	[19]
Cu^{2+}	Ash and zeolite	300	5	40	27.9	None	[41]

*Denotes experimental

ability to be desorbed and reused and thereby satisfying the demands of sustainability. The major difference in the production route between the current study and the pyrophyllite geopolymer adsorbent [18] is that the current study used activators (potassium aluminate) for synthesis of the geopolymer, whereas Panda et al. [18] only used sodium hydroxide. The curing regime was also different in that the FeCr-GP was cured at room temperature for 28 days, the GMT-GP was cured for 120 h at 100 °C, while the pyrophyllite geopolymer, the paste was agitated for 2 h at 100 °C and then left for strength development at room temperature for three days. The pyrophyllite geopolymer adsorption could be modelled using Langmuir and Temkin isotherm models, while the FeCr-GP and GMT-GP could be modelled using Langmuir isotherm model. Maleki et al. [40] also used sodium hydroxide with room temperature curing of the geopolymer, whose adsorption of a dye could be modelled using the Freundlich isotherm. Panda et al. [19] used sodium hydroxide and sodium silicate to produce a geopolymer from dolochar ash. The adsorption using this geopolymer could be modelled well using Langmuir isotherm. Harja et al.[41] used sodium hydroxide to synthesize a zeolite from coal ash with the adsorption of Cu modelled using pseudo-second-order kinetics.

CONCLUSION

Metal removal increased with solid loading, temperature and time for FeCr-GP and GMT-GP. Both geopolymers formed well buffered slurries with the synthetic water as the pH only increased from 2.3 to 4.8 within 240 min of adsorption. Metal removal was higher for FeCr-GP than GMT-GP due to the presence of calcium silicate hydrate (CSH) and calcium aluminate silicate hydrate (CASH). The adsorption process was endothermic for both geopolymers and the sorption process was physisorption. The presence of geopolymerization products in FeCr-GP allowed the geopolymer to have a saturation concentration of 400 ppm, while FeCr-GP without geopolymerization products had a saturation concentration of 200 ppm. Desorbed geopolymer property was dependent on the desorbing acid. For FeCr-GP H_2SO_4 resulted in the loss of CSH/CASH, resulting in reduced capacity for adsorption, whereas 0.1 M HCl did not affect the geopolymer property. GMT-GP could not be reused after desorption, as it resulted in a 17% and 39% decrease in metal removal efficiency with the use of 0.01 M HCl and 0.01 M H_2SO_4, respectively. This study therefore shows the importance of geopolymerization products in the adsorption property of a geopolymer adsorbent.

ACKNOWLEDGEMENTS

The author is grateful to the University of South Africa (UNISA) and the South African National Research Foundation for granting the primary author the DSI/NRF Freestanding Postdoctoral Fellowship.

AUTHORS' CONTRIBUTION

T Falayi supervised the experimental work and wrote the article. BD Ikotun supervised the laboratory work and approved the final manuscript.

FUNDING

The authors' research is funded by the South African National Research Foundation under the DSI/NRF Freestanding Postdoctoral Fellowship (PDG190226421150).

AVAILABILITY OF DATA AND MATERIALS

The datasets supporting the conclusions of this article are available in the supplementary material.

COMPETING INTERESTS

The authors declare that they have no competing interests.

SYMBOLS

Symbol

b : a constant related to Langmuir enthalpy of adsorption [L/g]
C_o : initial metal ion concentration (ppm)
C_t : metal ion concentration after t minutes of adsorption [ppm]
k_1 : pseudo first order constant [min^{-1}]
k_2 : pseudo second order constant [g/min·mg]
K_F : Freundlich constant related to adsorption intensity [L/mg]
n : Freundlich adsorption intensity
q_t : amount of metal ion adsorbed per mass of adsorbent after t minutes of adsorption [mg/g]
q_e : amount of metal ion adsorbed per mass of adsorbent at equilibrium of adsorption [mg/g]
q_m : maximum adsorption capacity
t : time [mins]

SUPPORTING INFORMATION

Additional information as noted in the text. This information is available via the Internet at http://www.springer.com/chemistry/journal/11814.

REFERENCES

1. M. Muller, *Water security in a Southern African context*, Springer Nature, Singapore (2018).
2. A. A. Siyal, M. R. Shamsuddin, N. E. Rabat, M. Zulfiqar, A. Man and A. Low, *J. Clean Prod.*, **229**, 232 (2019).
3. S. Chen, Y. Qi, J. J. Cossa and S. I. D. S Dos, *Prog. Nucl. Energy,* **117**, 103112 (2019).
4. M. Jaishankar, T. Tseten, N. Anbalagan, B. B. Mathew and K. N. Beeregowda, *Interdiscipl. Toxicol.*, **7**, 60 (2014).
5. F. J. López, S. Sugita, M. Tagaya and T. Kobayashi, *J. Mater. Sci. Chem. Eng.*, **2**, 16 (2014).
6. T. Falayi and F. Ntuli, *Korean J. Chem. Eng.*, **32**, 707 (2015).
7. T. Luukkonen, H. Runtti, M. Niskanen, E. T. Tolonen, M. Sarkkinen, K. Kemppainen, J. Ramo and U. Lassi, *J. Environ. Manage.*, **166**, 579 (2016).
8. A. Maleki, A. Hajizadeh, V. Sharifi and Z. Emdadi, *J. Clean Prod.*, **215**, 1233 (2019).
9. M. A. Memon, M. F. Nuruddin, S. Demie and N. Shafiq, *World Acad. Sci. Eng. Technol.*, **80**, 860 (2011).
10. S. A. Rasaki, A. Bingxue, R. Guarecuco, T. Thomas and Y. Minghui, *J. Clean Prod.*, **213**, 42 (2019).
11. P. Hua, L. Sellaouib, D, Francoc, M. S. Nettoc, G. L. Dottoc, A. Bajahzard, H. Belmabrouk, A. Bonilla-Petriciolet and L. Zichao, *Chem. Eng. J.*, **383**, 123113 (2020).
12. T. Luukkonen, A. Heponiemi, H. Runtti, J. Pesonen, J. Yliniemi and U. Lassi, *Rev. Environ. Sci. Biotechnol.*, **18**, 271 (2019).
13. T. Falayi, *Proc. Inst. Civ. Engin. - Wast. Res. Man.*, **172**, 56 (2019).
14. T. Falayi, *Sust. Envir. Res.*, **29**, 1 (2019).
15. T. R. Barbosa, E. L. Foletto, G. L. Dotto and S. L. Jahn, *Cer. Int.*, **44**, 416 (2018).
16. T. Luukkonen, K. Veznıkova, E. Tolonen, H. Runtti, J. Yliniemi, T. Hu, K. Kemppainen and U. Lassi, *Environ. Technol.*, **39**, 1 (2017).
17. Y. Liu, C. Yan, Z. Zhang, Y. Gong, H. Wang and X. Qiu, *Mater. Lett.*, **185**, 370 (2016).
18. L. Panda, S. S. Rath, D. S. Rao, B. B. Nayak, B. Das and P. K. Misra, *J. Mol. Liq.*, **263**, 428 (2018).
19. L. Panda, S. K. Jena, S. S. Rath and P. K. Misra, *Environ. Sci. Pollut. Res.*, **27**, 24284 (2020).
20. F. Demir and E. M. Derun, *J. Clean. Prod.*, **237**, 1 (2019).
21. Z. Zaheer, A. A. Aisha and E. S. Aazam, *J. Mol. Liq.*, **283**, 287 (2019).
22. H. M. F. Freundlich, *Z. Phys. Chem.*, **57**, 385 (1906).
23. J. Wang and X. Guo, *Chemosphere*, **258**, 127279 (2020).
24. G. McKay, Y. S. Ho and J. C. Y. Ng, *Sep. Purif. Methods*, **28**, 87 (1999).
25. S. S. Gupta and K. G. Bhattacharyya, *Adv. Colloid Interface Sci.*, **162**, 39 (2011).
26. X. Ren, L. Y. Zhang, D. Ramey, B. Waterman and S. Ormsby, *J. Mater. Sci.*, **50**, 1370 (2015).
27. J. Kiventera, L. Golek, J. Yliniemi and V. M. Ferreira, *Int. J. Min. Proc.*, **149**, 104 (2016).
28. J. A. Gadsden, *Infrared spectra of minerals and related inorganic compounds*, Butterworth, London (1975).
29. T. Bakharev, *Cem. Concr. Res.*, **35**, 1224 (2005).
30. A. Fernández-Jiménez and A. Palomo, *Cem. Concr. Res.*, **35**, 1984 (2005).
31. G. C. Allen and M. Paul, *Appl. Spectrosc.*, **49**, 451(1995).
32. M. J. Wilson, *Clay mineralogy: spectroscopic and chemical determinative methods*, Chapman & Hall, London (1994).
33. C. Navarro, M. Diaz and M. A. Villa-Garcia, *Environ. Sci. Technol.*, **44**, 5383 (2010).
34. F. Ntuli and A. E. Lewis, *Chem. Eng. Sci.*, **64**, 2202 (2009).
35. Z. Xiaolong, Z. Shiyu, L. Hui and Z. Yingliang, *J. Clean. Prod.*, **284**, 1 (2020).
36. S. K. Nath and S. Kumar, *Waste Biomass Valor.*, **10**, 2014 (2019).
37. S. K. Nath and S. Kumar, *Constr. Build. Mater.*, **125**, 127 (2016).
38. A. Hajimohammadi and J. S. J. van Deventer, *Int. J. Min. Proc.*, **153**, 80 (2016).
39. I. P. Okoye and C. Obi, *Int. Arch. Appl. Sci. Tech.*, **3**, 58 (2012).
40. A. Maleki, M. Mohammad, Z. Emdadi, N. Asim, M. Azizi and J. Safaei, *Arab. J. Chem.*, **13**, 3017 (2020).
41. M. Harja, G. Buema, D. Sutiman, C. Munteanu and D. Bucur, *Korean J. Chem. Eng.*, **29**, 1735 (2012).

Supporting Information

A comparison between ferrochrome slag and gold mine tailings based geopolymers as adsorbents for heavy metals in aqueous solutions: Analyzing reusability and sustainability

Thabo Falayi[†] and Bolanle Deborah Ikotun

Department of Civil and Chemical Engineering, University of South Africa, Johannesburg 1710, South Africa
(*Received 27 August 2020 • Revised 8 December 2020 • Accepted 14 December 2020*)

Effect of adsorbent dosage FeCr

	1st Run			2nd Run			3rd Run		
Adsorbent	Cu	Ni	Mn	Cu	Ni	Mn	Cu	Ni	Mn
0.1	80.54	78.65	90.25	81.23	80.77	89.99	80.33	77.78	90.88
0.2	70.66	60.54	88.25	69.33	59.77	85.76	70.84	60.77	88.12
0.3	20.56	40.45	70.28	19.66	41.23	69.25	20.56	41.01	70.12
0.4	1.54	12.66	23.76	1.65	12.78	23.67	1.56	12.33	24.77
0.5	0.88	3.45	10.67	0.87	3.21	11.66	0.9	3.42	10.16
0.6	0.87	0.65	1.67	0.88	0.66	1.88	0.87	0.67	1.89
0.7	0.8	0.64	0.92	0.8	0.66	0.95	0.8	0.67	0.96
0.8	0.8	0.66	0.93	0.7	0.67	0.95	0.7	0.63	0.96
0.9	0.8	0.63	0.94	0.8	0.67	0.94	0.8	0.63	0.96
1	0.79	0.63	0.92	0.8	0.67	0.94	0.81	0.66	0.96

Effect of adsorbent dosage (GMT)

	1st Run			2nd Run			3rd Run		
Adsorbent	Cu	Ni	Mn	Cu	Ni	Mn	Cu	Ni	Mn
0.1	86.78	90.67	95.33	88.76	92.67	94.56	86.78	90.41	94.66
0.2	60.33	80.67	89.07	62.67	79.88	90.67	60.78	80.89	89.98
0.3	20.45	60.54	70.77	18.88	55.76	69.08	20.37	54.33	70.41
0.4	12.66	40.55	55.67	11.98	39.88	54.9	12.63	40.78	55.09
0.5	5.67	20.55	34.55	4.67	22.13	36.88	5.08	22.56	36.88
0.6	1.54	12.56	15.56	1.67	10.65	15.78	1.98	12.89	14.95
0.7	0.85	2.85	8.89	0.88	1.66	10.84	0.89	1.78	11.45
0.8	0.84	1.78	2.78	0.85	1.05	3.98	0.9	1.13	4.12
0.9	0.84	0.85	0.95	0.85	0.9	1.88	0.9	0.88	1.67
1.0	0.83	0.85	0.88	0.85	0.9	0.9	0.9	0.89	0.91
1.2	0.83	0.85	0.88	0.85	0.9	0.9	0.9	0.87	0.91
1.4	0.83	0.85	0.88	0.85	0.9	0.9	0.9	0.88	0.9

Saturation

	1st Run			2nd Run			3rd Run		
Initial con	Cu	Ni	Mn	Cu	Ni	Mn	Cu	Ni	Mn
100	0.8	0.66	0.96	0.8	0.66	0.96	0.8	0.66	0.96
200	1.2	2.5	6.77	1.12	2.45	5.78	1.2	2.88	6.88
300	2.3	3.5	8.98	2.45	3.88	8.99	2.3	4.02	8.65
400	2.5	5.67	10.89	2.6	5.78	12.67	2.5	5.23	12.65
500	102.5	110.78	120	101	110.78	123	98.99	115	121
600	202.45	220.56	233.67	210	218.56	238	199.78	212	233

GMT

	1st Run			2nd Run			3rd Run		
Initial con	Cu	Ni	Mn	Cu	Ni	Mn	Cu	Ni	Mn
100	0.86	0.88	0.896667	0.86	0.88	0.896667	0.86	0.88	0.896667
200	2.89	2.5	6.77	1.12	2.45	5.78	1.2	2.88	6.88
300	112	145	133	134	132	135	112	142	144
400	255.65	266	288	252	270	12.67	244	266	267

Effect of T FeCr-GP (Cu)

		0	30	60	90	120	150	180	210	240
1	Cu	400	35	12.5	5	2.533333	1.87	1.86	1.87	1.87
2		400	38	11.5	6.5	2.5333	1.88	1.88	1.87	1.87
3		400	38	11.8	5	2.53	1.88	1.87	1.87	1.87

	0	30	60	90	120	150	180	210	240
Cu	400	10.44	5.65	3.2	1.32	0.98	0.95	0.95	0.95
	400	10.33	4.23	3.6	1.44	0.97	0.96	0.97	0.95
	400	10.65	5.25	3.8	1.38	0.98	0.95	0.98	0.96

	0	30	60	90	120	150	180	210	240
Cu	400	8.67	1.42	0.97	0.55	0.5	0.53	0.51	0.51
	400	8.98	1.34	0.98	0.55	0.55	0.54	0.52	0.54
	400	8.12	1.78	0.98	0.56	0.52	0.55	0.54	0.55

Ni

		0	30	60	90	120	150	180	210	240
1	Ni	400	101.23	20.65	8.56	5.56	5.23	5.33	5.34	5.67
2		400	101.45	20.34	9.12	5.56	5.36	5.78	5.33	5.34
3		400	100.34	20.87	9.62	5.56	5.34	5.78	5.66	5.34

	0	30	60	90	120	150	180	210	240
Ni	400	70.25	15.68	6.32	3.23	3	3.14	3.55	3.2
	400	71.54	15.18	6.91	3.12	3.17	3.98	3.16	3.4
	400	70.76	15.91	6.01	3.77	3.23	3.21	3.55	2.99

	0	30	60	90	120	150	180	210	240
Ni	400	50.38	10.33	3.45	3.12	2.97	3.29	3.22	3.16
	400	48.54	10.87	3.66	3.13	3.2	3.17	3.17	3.16
	400	48.99	10.59	3.86	3.16	3.12	3.28	3.15	3.17

Mn

	0	30	60	90	120	150	180	210	240
Mn	400	150	100.24	60.54	12.07	12.12	12.11	11.89	11.98
	400	150.23	100.45	60.67	12.07	12.054	12.19	11.99	12.1
	400	148.56	100.66	60.98	12.07	12.13	11.98	12	12.09

	0	30	60	90	120	150	180	210	240
Mn	400	135.77	98.34	33.55	8.78	5.77	5.78	5.75	5.46
	400	142.78	98.33	33.87	8.19	5.93	5.87	5.89	5.83
	400	133.89	97.92	33.45	8.15	5.67	5.66	5.44	5.99

	0	30	60	90	120	150	180	210	240
Mn	400	98.36	20.45	10.56	3.56	3.12	3.81	3.12	3.19
	400	97.13	20.51	10.62	3.89	3.23	3.12	3.44	3.17
	400	98.77	22.56	10.93	3.56	3.88	3.17	3.81	3.18

Effect of T on GMT-GP
Cu

	0	30	60	90	120	150	180	210	240
Cu	200	42.37	14.66	7.89	1.736667	1.62	1.64	1.58	1.58
	200	42.64	14.88	7.97	1.736667	1.63	1.62	1.57	1.55
	200	39.66	14.83	7.12	1.736667	1.64	1.59	1.52	1.56

0	30	60	90	120	150	180	210	240
200	20.56	9.98	3.56	1.12	1.08	1.1	1.03	1
200	20.67	9.78	3.44	1.13	1.05	1.05	1.04	1.03
200	18.54	9.77	3.88	1.12	1.12	1.04	1.08	1.06

0	30	60	90	120	150	180	210	240
200	10.66	4.34	1.88	0.87	0.65	0.65	0.66	0.66
200	10.34	4.23	1.67	0.81	0.62	0.7	0.6	0.62
200	10.89	4.67	1.78	0.91	0.67	0.65	0.7	0.61

Ni

	0	30	60	90	120	150	180	210	240
Ni	200	60.56	33.56	8.48	2.61	2.59	2.57	2.57	2.54
	200	60.32	27.59	8.42	2.61	2.57	2.54	2.57	2.61
	200	61.34	31.56	8.89	2.61	2.5	2.59	2.57	2.56

	0	30	60	90	120	150	180	210	240
Ni	200	45.32	15.23	4.56	2.1	2.13	2	2	2.08
	200	44.56	14.97	4.66	2.23	2.19	1.99	1.99	1.99
	200	43.67	15.34	4.89	2.15	2.17	2.12	1.99	1.98

	0	30	60	90	120	150	180	210	240
Ni	200	23.4	8.34	1.45	1.42	1.55	1.34	1.38	1.34
	200	22.89	9.12	1.56	1.83	1.67	1.37	1.37	1.34
	200	23.7	8.67	1.48	1.55	1.45	1.38	1.34	1.36

Mn

	0	30	60	90	120	150	180	210	240
Mn	200	88.34	22.24	13.56	6.476667	6.34	6.27	6.3	6.32
	200	89.45	22.44	13.83	6.476667	6.34	6.32	6.32	6.33
	200	88.14	22.32	13.67	6.476667	6.12	6.38	6.31	6.3

	0	30	60	90	120	150	180	210	240
Mn	200	51.56	22.34	10.78	4.67	4.56	4.32	4.56	4.4
	200	51.66	22.63	10.68	4.87	4.34	4.78	4.33	4.34
	200	51.78	22.67	10.55	4.32	4.23	4.56	4.38	4.42

	0	30	60	90	120	150	180	210	240
Mn	200	28.78	9.89	3.21	3.26	3.2	3.1	3.09	3.08
	200	28.12	9.98	3.23	3.26	3.2	3.1	3.08	3.09
	200	28.36	9.77	3.33	3.28	3.2	3.1	3.09	3.09